SLAC-PUB-925
June 1971
(TH) and (EXP)

HIGH ENERGY π^0 PHOTOPRODUCTION FROM HYDROGEN WITH UNPOLARIZED AND LINEARLY POLARIZED PHOTONS*

R. L. Anderson, D. B. Gustavson, J. R. Johnson, I. D. Overman
D. M. Ritson and B. H. Wiik
Stanford Linear Accelerator Center
Stanford, California

D. Worcester+
Harvard University
Cambridge, Massachusetts

Abstract

We have completed measurements of the differential cross section for $\gamma + p \rightarrow \pi^0 + p$, and the asymmetry with polarized photons, for incident photon energies from 4 to 18 GeV and momentum transfers between t=-0.1 and $-1.4(\mathrm{GeV}/c)^2$. The experiment was performed at the Stanford Linear Accelerator Center, using the SLAC 1.6 GeV/c spectrometer to analyze protons recoiling from a hydrogen target. For the cross section measurements a normal collimated bremsstrahlung beam was used. For the asymmetry measurements the polarized photons were produced by coherent bremsstrahlung from a diamond crystal, and a coincidence was required between the recoil proton and one of the π^0 decay photons in a shower counter.

(Submitted for publication)

---

*Work support by the U.S. Atomic Energy Commission

+Present address: Daresbury Nuclear Physics Lab., Lancashire, England.

Introduction

The π^o photoproduction process at high energies and small momentum transfers has been subject to much experimental and theoretical work over the past few years[1]. Measurements of the cross section and the asymmetry with polarized photons have been made at DESY[2] and CEA[3] for incident energies below 5.8 GeV. These measurements have been extended up to 15 GeV at SLAC[4,5]. The most prominent feature of the differential cross section is the dip at a four-momentum transfer squared of $t \approx -.5(\mathrm{GeV/c})^2$, plus a weak but significant shrinkage with increasing energy for $|t| \leq 1.4(\mathrm{GeV/c})^2$. The results from the SLAC experiment[4] seemed to indicate that the dip, although present at all energies, became less pronounced with increasing photon energy. However, since the SLAC experiment only measured the sum of the cross sections for Compton scattering and π^o production, the cross section in the dip region was strongly dependent upon the Compton correction used and therefore rather uncertain.

The observed asymmetry[3,5] with polarized photons on the proton at 3 and 6 GeV showed a large positive asymmetry with indications of a dip near $t \approx -.5(\mathrm{GeV/c})^2$. In addition to the data on the proton, some preliminary results for the cross section on the neutron at 4 GeV are available[1]. The ratio of the neutron to the proton cross section is again close to 1 with an apparent dip at $t = -.5(\mathrm{GeV/c})^2$.

Within the framework of the Regge model these data must be explained by Reggeized ρ, ω, and B-exchange in the t-channel. In a conventional Regge[6] model with wrong signature nonsense zeros the contributions from the ρ and the ω-trajectory will disappear for $t = -.5(\mathrm{GeV/c})^2$ and the observed dip must be filled up by B-exchange. Assuming the usual slope of $\sim 1(\mathrm{GeV/c})^2$ the B-trajectory will have an intercept at $t = 0$ of about $-.3$ as compared to

about +.5 for the ρ and the ω-trajectory. Therefore in such a conventional Regge model with nonsense zeros we would expect the observed dip in the cross section to grow deeper with increasing photon energy and the cross section at the dip to be dominated by unnatural parity exchange. Both predictions are in contradiction to the experimental findings and a conventional Regge model can therefore not fit the data. To fit the data we have to include absorption[7,8,9,10] in the Regge model or assume that either the trajectories[11] or the residue functions[12] associated with ρ and ω-exchange are different.

This experiment extended our previous differential cross section measurements down to small t-values, to a region where the absorptive corrections should be relatively small. At the time of our first publications the data were corrected for the Compton contribution using a theoretical estimate for this cross section. We have re-evaluated all these earlier data using the now known Compton cross section. Furthermore, as a consistency check we include the results of a coincidence measurement in the critical region around $t = -.5(\text{GeV/c})^2$ for an incident photon energy of 17 GeV. This paper therefore supercedes our previous publications and contains our final data on the differential cross section between 4 and 15 GeV and for t-values in the range from $-.1(\text{GeV/c})^2$ to $-1.4(\text{GeV/c})^2$. The second part of this paper contains our measurements of the asymmetry in π^o photoproduction on the proton with linearly polarized photons for incident photon energies of 4, 6, and 10 GeV and for t-values in the range from $-.2(\text{GeV/c})^2$ to $-1.4(\text{GeV/c})^2$. A preliminary report on a part of the 6 GeV results has been published previously[5].

Differential Cross Sections

The method and apparatus have been described in considerable detail

elsewhere[4,13]. The experimental layout is shown in Fig. 1. A collimated bremsstrahlung photon beam from the SLAC accelerator was passed through a hydrogen target and stopped downstream in a secondary-emission quantameter (SEQ), our primary beam monitor. This SEQ was frequently calibrated against a silver calorimeter, using a Cerenkov monitor as the intermediate standard. The yield of protons recoiling from the target was measured as a function of laboratory angle for various recoil momenta and incident beam energies, using the SLAC 1.6 GeV/c spectrometer. This is a 90° bend (254cm radius), second-order corrected, weak-focusing magnet in which momentum and production angle of the incident charged particles are focused in a single plane normal to the central flight path.

A gaseous hydrogen target was used for $|t| \leq 0.4(\mathrm{GeV/c})^2$ because the lower limit on momentum transfers we could observe was set by multiple scattering and range of the low momentum recoil protons. To avoid too great a reduction in counting rate, the target cell was cooled to about 37°K and filled to a pressure of approximately 120 psi, giving a hydrogen density of 0.01 $\mathrm{gm/cm^3}$. The cell wall facing the spectrometer had a 0.025 cm thick mylar window , and the scattering chamber was connected directly to the spectrometer vacuum. Thus the amount of material between the center of the target and the exit of the spectrometer vacuum was reduced to 0.002 radiation length.

Protons were identified by pulse height in a series of backing counters together with a veto on pions (for $|t| \geq 0.4(\mathrm{GeV/c})^2$) from a lucite threshold Cerenkov counter. The proton trigger was then put in coincidence with a "missing-mass hodoscope" of eight counters in the spectrometer focal plane, each 25 cm × 1.9 cm × 0.6 cm thick. The first two backing counters, before the hodoscope, were only 0.08 cm thick, while the others were 1.25 cm thick.

The hodoscope elements were rotated about the central flight path to align with (p,θ) lines of constant threshold missing-mass according to the equation

$$MM^2 = 2 E_o (p \cos \theta - T) = 2 M_p T$$

where p, θ, T are the proton momentum, production angle, and kinetic energy, and E_o is the beam end-point energy.

With a bremsstrahlung beam and fixed spectrometer field, the proton rate across the hodoscope will show a step at the threshold for production of a single neutral particle such as π^o. An example is shown in Fig. 2. The lines show a least-squares fit assuming smooth backgrounds from "ghost protons" and multipion production. The π^o step heights so obtained were converted to cross sections taking into account the spectrometer acceptance, beam monitor calibrations, and various corrections. The total correction was typically between 10 and 20%, and the overall normalization uncertainty is about 5%. Since the experimental resolution was not sufficient to separate π^o photoproduction from proton Compton scattering, it was necessary to make a further correction by subtracting the appropriate Compton contribution. For previous publications, only estimates of this contribution were available, but we have since made high-energy measurements of the Compton effect[14] using a coincidence technique. The same systematic errors appear in both measurements, so the subtraction is particularly reliable.

Fig. 3 shows final π^o photoproduction cross sections measured at a particular momentum transfer, $t = -0.7(\text{GeV}/c)^2$, with $d\sigma/dt$ in $\mu b/(\text{GeV}/c)^2$ plotted versus incident energy in GeV, both scales logarithmic. A straight-line fit was made for each t-value, of the form $d\sigma/dt \sim (s-M_p^2)^{2\alpha(t)-2}$, to

extract the effective Regge trajectory. In every case the fit was very good, and the solid line in Fig. 3 is an example.

The effective α values so obtained are plotted versus $|t|$ in Fig. 4. The points at high $|t|$ are not in agreement with expectations based on dominant ω-exchange, which should give $\alpha(t) = \alpha_\omega(t) \approx 0.45 + 0.9t$, shown as the dashed line in the figure. The weak shrinkage observed is consistent with linear behavior, and a least-squares fit gives an intercept $\alpha(0) = (0.184 \pm 0.034)$ and a slope of $(0.265 \pm 0.039)\ (\mathrm{GeV/c})^{-2}$. However, the values are also consistent with a larger slope at small $|t|$ and a much smaller slope at large $|t|$, as predicted by models including cuts or absorption. As an example, the solid curve shows the model of Frøyland[8].

As mentioned above, the fits $d\sigma/dt \sim (s-M_p^2)^{2\alpha-2}$ provide a good representation of the data. To produce angular distributions at standard energies, and as an average over the numerous individual points, values of $d\sigma/dt$ were taken from these straight-line fits at fixed values of E_o = 6, 9, 12, and 15 GeV. The results are listed in Table I and plotted in Fig. 5. The distributions show a "dip" around $t = -0.5(\mathrm{GeV/c})^2$, not changing much with energy. The slight change from our earlier publications is due to the improved subtraction of the Compton contribution. The extracted π^o cross section in the dip depends very critically on this correction. For example, at 15 GeV and $t = -.5(\mathrm{GeV/c})^2$ two-thirds of the observed yield is due to Compton scattering. Whereas we earlier had to rely upon a theoretical estimate for this correction, experimental values can now be used directly. It is important to note that the experimental setup was nearly the same for the two experiments, hence there are practically no systematic errors attached to this correction. However, since the dip region at the highest energies is difficult to fit and requires such a large Compton subtraction, we have

made coincidence measurements using the technique described in the next section (but with unpolarized photons). Fig. 6 shows coincidence yields across the hodoscope at 17 GeV average photon energy and momentum transfers both in the dip and on the secondary maximum, where single-arm measurement is fairly easy. It is clear that the π^o cross section does not vanish at $t = -0.5(\text{GeV/c})^2$, and in fact the coincidence result is in very good agreement with the single-arm results in Fig. 5.

Since the α-values in Fig. 4 are near zero, multiplying the cross section by $(s-M_p^2)^2$ removes most of the energy dependence. Fig. 7 shows our 4 and 6 GeV points compared in this manner with results from DESY. The agreement is very good, even though the experiments use different methods.

Asymmetry with Polarized Photons

Measurements of π^o photoproduction with linearly polarized photons provide additional information about the process, since they allow the separation of the natural and unnatural parity exchanges to leading orders of (t/s)[15]. The asymmetry is defined as $A = \frac{\sigma_\perp - \sigma_\parallel}{\sigma_\perp + \sigma_\parallel}$ where $\sigma_\perp(\sigma_\parallel)$ is the cross section with photons polarized normal (parallel) to the reaction plane. Trajectories with a natural parity sequence (ω,ρ) will contribute only to $\sigma_\perp$, whereas trajectories with unnatural parities (B) will contribute only to $\sigma_\parallel$. Absorption or cuts are in general expected to make contributions to both.

In this experiment we have made measurements with polarized photons for $0.2 \leq |t| \leq 1.4(\text{GeV/c})^2$ and average energies 4, 6, and 10 GeV. The layout is shown in Fig. 8. A narrow, parallel electron beam was steered onto a 0.1cm thick diamond crystal mounted in a goniometer, producing coherent bremsstrahlung. The electrons were swept away and the photons con-

tinued along the same beam line described in the previous section. The process was determined by a coincidence between the recoil proton detected in the 1.6 GeV/c spectrometer and one of the γ's from the π^{o} decay observed by one of the two lead-lucite shower counters, as described below.

The goniometer for the diamond was constructed and installed at SLAC by L. Osborne, D. Luckey, and R. Schwitters. It permits rotations around two perpendicular axes in well defined steps of 2.32×10^{-5} radians. To align the diamond with respect to the electron beam we used the method proposed by Luckey and Schwitters[16]. This method is based upon the fact that the ratio of the number of photons in the beam to the total power in the beam increases rapidly as the energy of the leading edge of a major spike in the spectrum approaches zero. In our case, this ratio was determined by the ratio of the Cerenkov monitor to the SEQ. Hence by measuring this ratio we efficiently determined the whole lattice map of the diamond. From the lattice map we can uniquely predict the position of the goniometer to obtain a required spectrum. To check the bremsstrahlung spectrum and our positioning of the diamond we measured the spectrum for both polarizations using the SLAC pair spectrometer[17] at 0^{o}. The incident electron energy was 12 GeV, and the polarized spike was set at 6 GeV. The measured spectra as shown in Fig. 9a were the same within statistics and were in good agreement with the computed spectrum[18]. The polarization corresponding to the computed spectrum is shown in Fig. 9b.

At the beam levels used in this experiment ($\lesssim$ 1ma) no changes in the lattice map due to heating of the crystal or its holder were observed. We therefore assume that the computed spectrum represents the true spectrum under data taking conditions. To minimize systematic errors, approximately every half hour the polarization was switched and the position of the diamond was checked. The reproducibility was excellent and the observed changes in

the position of the polarized spike were generally consistent with no change and never larger than 2% (corresponding to $\leq$ 3% change in beam polarization).

The photons from the π^o decay were detected in two shower counters, one above and the other below the reaction plane. The arrangement of the counters is shown in detail in the insert of Fig. 8. Each was 60cm long, 30cm high, and about 13 radiation lengths thick. The counters were placed inside a well shielded cave, which could be moved remotely in angle and height. The distance from the target was approximately 18 meters. The acceptance in horizontal angles $\Delta\theta$ of the shower counter was defined by remotely moveable slits, and $\Delta\theta/\theta$ (note $\Delta k/k \sim \Delta\theta/\theta$) was kept constant during the experiment. To reduce the pileup from low energy photons, 2 radiation lengths of carbon was put in front of the counters. To avoid counting Compton events, the counters were placed a distance above and below the reaction plane defined by the incoming photon and the recoil proton. In Compton scattering the scattered photon is in this plane, whereas the π^o decays into two photons with a typical opening angle of m_π/E_π. The required distance between the π^o counters is then given by the azimuthal acceptance of the proton spectrometer including multiple scattering. The geometry of the counters was such that only one of the photons could be detected, hence the outputs from the two counters were simply added linearly. A third counter (labeled "Compton counter") and accompanying slits were placed behind the π^o counters to accept the Compton events, for a separate experiment. To check alignment of the system and performance of the counters, we could remove the diamond, turn off the sweep magnets, and do elastic e-p scattering, for which the rates were good and the backgrounds low.

In the π^o measurement the t-value as well as the photon energy k was defined by the recoil proton, with the shower counter acting as an approxi-

mately one-third efficient device. To make sure that the background was negligible we moved the shower counters down below the π^o decay cone. After subtraction of the accidentals, the coincidence rate out of the "plane" was $(-9 \pm 11)\%$ of the coincidence rate in the plane. We therefore subtracted only the accidental counts (typically about 20%) and no background from the coincident events. Since the background events are presumably less asymmetric than π^o production, this procedure would lead to a lower limit for the resulting asymmetry. The same conclusion holds if the beam were degraded in some undetected way, resulting in a lower actual polarization than that assumed in the analysis.

In Fig. 10 the true coincidence rate between the π^o shower counter and the proton is plotted for the photon polarized normal to and parallel to the reaction plane, for $\bar{E} = 6$ GeV and $t = -.8(\mathrm{GeV/c})^2$. The results at other energies and t-values are similar. The photon energy as defined by the recoil proton is indicated on the drawing. For all 6 GeV measurements the leading edge of the polarized spike was set at 6.74 GeV; the other energies were set similarly. The shape of the solid curve was derived using the computed photon spectrum, folding in the multiple scattering of the proton and the acceptance of the shower counter. The height was then adjusted to give agreement with the data. To determine the asymmetry in this case only hodoscope elements 4 - 8 were used. The average polarization over the useful part of the photon spectrum was $\sim 50\%$ for 6 and 10 GeV, and $\sim 70\%$ for 4 GeV.

The asymmetries extracted from these data are plotted in Fig. 11 versus t, together with the earlier results[3] from CEA and a theoretical prediction by Frøyland[8]. Only the statistical error is plotted. In addition we have an estimated systematic error of about 5% resulting from uncertainties in

determining the photon energy and computing the polarization of the photon beam. The results are consisted with no energy dependence. The points all show high positive asymmetry, as expected from a strongly dominant natural parity exchange in the t-channel. If B-exchange were dominant near $t = -0.5(\text{GeV}/c)^2$, the small dip seen there would have to extend well into the negative asymmetry region. Thus the data are strongly in disagreement with such a model. Also models[11] which explain the differential cross section data by assuming different trajectories for the ρ and the ω fail to reproduce the asymmetry data. Models including cuts or absorption, of which Fröyland's is an example, clearly can achieve reasonable agreement with the experiment.

Combining the 6 GeV asymmetries with the corresponding differential cross sections from the previous section, one can extract separate contributions from the two polarizations. The results are shown in Fig. 12. All the structure appears to be in $\sigma_\perp$.

Discussion

Since the relative size of the cross section in the dip region remains constant independent of energy, and the ratio of natural to unnatural parity exchange is large and independent of energy even in the dip region, we conclude that B-exchange is unimportant in π^o photoproduction. Neglecting B-exchange, a comparison of the coupling constants involved in ρ and ω-exchange shows that the process should be dominated by ω-exchange with some contribution from ρ-exchange. In addition to the pole exchanges, absorption or cuts must be included.

Formally the polarized photon cross sections can be analyzed in terms of the s or t-channel helicity amplitudes. Defining the s-channel helicity amplitudes $f_{\lambda\mu}$, where λ denotes the final and μ the initial proton helicity

and the photon helicity is always set equal to 1, the asymmetry A with linearly polarized photons can be written as:

$$A = 2R_e \frac{(f_{1/2,1/2} \cdot f^*_{-1/2-1/2} - f^*_{1/2-1/2} \cdot f_{-1/2,1/2})}{|f_{1/2,1/2}|^2 + |f_{-1/2-1/2}|^2 + |f_{1/2-1/2}|^2 + |f_{1/2,1/2}|^2}$$

In terms of only ρ and ω-exchange we have:

$$f_{1/2,1/2} = f_{-1/2-1/2} \quad \text{and} \quad f_{1/2-1/2} = -f_{-1/2,1/2}$$

In the presence of cuts or absorption the first relationship remains true but $f_{1/2-1/2}$ is no longer equal to $f_{-1/2,1/2}$. Hence in general we would expect A to be different from 1 in the presence of absorption. Since A is very close to 1 at large t-values where absorption dominates, we interpret this result to show that $f_{1/2,1/2} \simeq f_{-1/2-1/2}$ and that both $f_{1/2-1/2}$ and $f_{-1/2,1/2}$ must be small[19]. Translated back into the t-channel, this then relates the non-spin flip amplitude to the spin flip amplitude requiring both to be large at large values of $|t|$.

Good fits to the present available data in π^o photoproduction can be achieved with a variety of models, all of which include cuts or absorption in some form. In both the strong absorption model[9] and the Dar-Weisskopf[10] model the Regge exchange amplitude contains no wrong signature nonsense zero. In the strong absorption model the dip is caused by destructive interference between the pole and the cut terms. In the Dar-Weisskopf model each helicity amplitude is dominated by the most peripheral wave. This leads to an amplitude proportional to $J_{\Delta\lambda}(\sqrt{-t}R)$, where $J_{\Delta\lambda}$ is a Bessel function of order $\Delta\lambda$ and R is the interaction radius. $\Delta\lambda$ is the total s-channel helicity flip. From the above discussion it is clear that the cross section will be dominated by the $\Delta\lambda = \pm 1$ amplitudes, corresponding to a dip in the cross section around

$t = -.5(\mathrm{GeV}/c)^2$ for a typical interaction radius of 1fm. In the weak cut models[8], the observed structure is directly related to the wrong signature nonsense zero at $t = -.5(\mathrm{GeV}/c)^2$ for the ρ and ω contribution, and the cross section at the dip is given by the cut contribution.

All these models, although their individual amplitudes are quite different in the different models, give good fits to the present available data in π^0 photoproduction. However none of these models describe all inelastic reactions properly[20]. One of the short-comings of these models is that they only incorporate Regge-Pomeron cuts in addition to the primary Regge pole exchange. However measurements of the ratio $\frac{(\gamma P \to \pi^+ \Delta^0) + (\gamma N \to \pi^+ \Delta^-)}{\gamma P \to \pi^+ \Delta^0}$ have shown that at 16 GeV, I=2 exchanges contribute about 20% of the amplitude. The observed I=2 exchanges can be explained by double particle exchange[21], and it is expected that such exchanges would be even more important at lower energies. Since double particle exchanges have been neglected in all theories, the good agreement between theory and experiment may be fortuitous, and we consider it quite remarkable that the observed behavior for large t-values is consistent with only natural parity exchange.

Acknowledgement

We wish to thank A. Schwimmer for many helpful discussions. J. Grant, E. Cheatham and J. Schroeder gave us invaluable support with the setup and the preparation for the experiment. We wish to acknowledge the help we received from the Operations Group and the Spectrometer Facilities Group at SLAC, and in particular we wish to thank R. Miller and A. Golde.

REFERENCES

1. For a review see: K. Lübelsmeyer, in Proceedings of the Fourth International Symposium on Electron and Photon Interactions at High Energies, Daresbury Nuclear Physics Laboratory, Liverpool, England, 1969, edited by D. W. Braben (Daresbury Nuclear Physics Laboratory, Daresbury, Lancashire, England (1970)).
2. M. Braunschweig et al., Phys. Letters 26B, 405 (1968).
3. D. Bellinger et al., Phys. Rev. Letters 23, 540 (1969).
4. R. L. Anderson et al., Phys. Rev. D1, 27 (1970).
5. R. L. Anderson et al., Phys. Rev. Letters 26, 30 (1971).
6. A. P. Ader, M. Capdeville, and Ph. Salin, Nuclear Physics B3, 407 (1967).
7. Models that involve the B in addition to $\omega(\rho)$ and absorption:
   M. L. Blackmon, G. Kramer, and K. Schilling, Phys. Rev. 183, 1452 (1969).
   M. Biyajima and M. Kemmaku, Progress of Theoretical Physics 43, 1255 (1970).
8. Models with $\omega(\rho)$ and cuts, "weak absorption model":
   J. Fröyland, Nuclear Physics B11, 204 (1969).
   A. Capella and J. Tran Thanh Van, Nuovo Cimento Letters 1, 321 (1969).
   P. Contogouris and J. P. Lebrun, Nuovo Cimento 64A, 627 (1969).
   G. Benefatto et al., Nuovo Cimento 64A, 1033 (1969).
9. "Strong absorption model":
   G. L. Kane et al., Phys. Rev. Letters 25, 1519 (1970).
   R. A. Miller, Phys. Rev. D2, 598 (1970).
   M. Colocci, Nucovo Cimento Letters 4, 53 (1970).
10. A. Dar, T. L. Watts, and V. F. Weisskopf, Physics Letters 30B, 264 (1969).
11. R. P. Bajpai and A. Donnachie, Phys. Letters 30B, 344 (1969).
12. C. B. Chiu and S. Matsuda, Phys. Letters 31B, 455 (1970).
    G. Kramer, Private Communication.

13. J. R. Johnson, SLAC Report No. 124 (1970).

14. R. L. Anderson et al., Phys. Rev. Letters 25, 1218 (1970).

15. P. Stichel, Z. Physik 180, 170 (1964).

16. D. Luckey and R. F. Schwitters, Nucl. Instr. and Methods 81, 164 (1970).

17. A. Boyarski et al., (to be published).

18. We thank Roy Schwitters for the computer program.

19. This observation is consistent with the assumption that ω-exchange in the t-channel conserves the s-channel nucleon helicity. Other experimental evidence in favor of s-channel nucleon helicity conservation in ω-exchange has been discussed by Odorico et al., in Phys. Letters 32B, 375 (1970).

20. H. Harari, Phys. Rev. Letters 26, 1400, (1971).

21. C. Quigg, Thesis, University of California, Berkeley.

H. Harari, Phys. Rev. Letters 26, 1079 (1971).

F. S. Henyey et al., Preprint from the University of Michigan, Ann Arbor, Michigan (1970).

TABLE I

$d\sigma/dt \quad (\gamma + p \rightarrow \pi^0 + p)$, $\mu b/(GeV/c)^2$

$\|t\|$, $(GeV/c)^2$	E_0 = 6 GeV	E_0 = 9 GeV	E_0 = 12 GeV	E_0 = 15 GeV
.1	1.13 ± .11	.59 ± .07	.37 ± .05	
.15	.86 ± .06	.47 ± .05	.30 ± .04	.22 ± .03
.2	.67 ± .05	.33 ± .04	.20 ± .03	.137 ± .020
.3	.34 ± .04	.138 ± .020	.073 ± .013	.045 ± .009
.4	.130 ± .014	.058 ± .008	.033 ± .006	.021 ± .005
.5	.078 ± .010	.039 ± .006	.024 ± .004	.016 ± .003
.6	.095 ± .012	.045 ± .008	.027 ± .006	.018 ± .004
.7	.122 ± .010	.054 ± .005	.030 ± .003	.019 ± .003
.8		.066 ± .013	.038 ± .003	.024 ± .003
.9	.140 ± .007	.063 ± .004	.036 ± .003	.0231 ± .0025
1.1	.129 ± .005	.051 ± .003	.027 ± .002	.0160 ± .0013
1.38	.0849 ± .0045	.0321 ± .0024	.0161 ± .0013	.0094 ± .0009

TABLE II

$$A = \frac{\sigma_{\perp} - \sigma_{\parallel}}{\sigma_{\perp} + \sigma_{\parallel}}$$ (errors are statistical)

$\lvert t \rvert$ $(\mathrm{GeV}/c)^2$	$\bar{E}$, GeV: 4	6	10
0.2	.91 ± .05	.87 ± .08	.88 ± .15
0.3	.83 ± .04	.81 ± .09	
0.4	.77 ± .045	.79 ± .085	.62 ± .15
0.5	.69 ± .05	.69 ± .11	
0.6	.78 ± .04	.72 ± .06	.78 ± .08
0.7	.82 ± .035	.79 ± .11	
0.8	.79 ± .035	.92 ± .07	.90 ± .065
0.9	.93 ± .03	.84 ± .09	
1.0	.82 ± .05	.95 ± .07	.93 ± .06
1.1	.88 ± .03	.93 ± .07	
1.2	.91 ± .03	.90 ± .06	.91 ± .055
1.3	.96 ± .035	.89 ± .06	
1.4	.99 ± .03	.96 ± .055	.99 ± .055

FIGURE CAPTIONS

Fig. 1: Experimental arrangement for measurement of π^o photoproduction cross sections.

Fig. 2: The observed proton yield, in counts per hodoscope element per 10^{12} equivalent quanta, is plotted versus (missing mass)^2 in the vicinity of the π^o threshold. The photon end-point energy is 6 GeV, and $t = -0.5(\text{GeV/c})^2$ in (a) and $-1.1(\text{GeV/c})^2$ in (b).

Fig. 3: For $t = -0.7(\text{GeV/c})^2$, $d\sigma/dt$ in $\mu b/(\text{GeV/c})^2$ is plotted versus photon energy in GeV, with both scales logarithmic. The solid line is a fit of the form $d\sigma/dt \sim E_o^{2\alpha-2} \sim (s-M_p^2)^{2\alpha-2}$ and the value of α is shown.

Fig. 4: Values of the effective α are plotted versus $|t|$. The dashed line indicates the $\alpha(t)$ expected for pure ω-exchange. The solid line is from the model of Fröyland.

Fig. 5: $d\sigma/dt$ in $\mu b/(\text{GeV/c})^2$ is plotted versus $|t|$ for incident photon energies of 6, 9, 12, and 15 GeV. The dashed lines are only to guide the eye.

Fig. 6: Shown are proton yields in the hodoscope, in coincidence with π^o decay photons in a shower counter. The units are counts per hodoscope element per 10^{14} equivalent quanta, plotted versus hodoscope number. The average photon energy is 17 GeV and two momentum transfers are represented: $t = -0.8(\text{GeV/c})^2$ and $t = -0.5(\text{GeV/c})^2$.

Fig. 7: Results from this experiment, expressed as $(s-M_p^2)^2\, d\sigma/dt$ in $\mu b/(\text{GeV/c})^2$, are plotted versus $|t|$ together with measurements from DESY for comparison.

Fig. 8: Experimental arrangement for measurement of the asymmetry in π^o photoproduction with polarized photons.

Fig. 9: (a) Shown is the intensity spectrum of coherent bremsstrahlung from the diamond used in this experiment, as measured by the SLAC pair spectrometer. The points were taken with the diamond oriented to give photons polarized normal to the reaction plane. The solid curve is a theoretical spectrum fitted to the measurements with polarization parallel to the reaction plane. (b) The solid curve shows the beam polarization corresponding to the computed spectrum in (a).

Fig. 10: Spectrometer shower counter coincidence yields from a coherent bremsstrahlung beam are plotted versus hodoscope number. The spectrometer was set for $t = -0.8(\mathrm{GeV}/c)^2$, and the edge of the coherent spike in the beam was set at 6.74 GeV with an incident electron energy of 12 GeV. The photon energy variation across the hodoscope is indicated by the arrows.

Fig. 11: The measured asymmetry at 4, 6, and 10 GeV average photon energies is plotted versus $|t|$. Measurements at 3 GeV by the MIT group are included for comparison. The solid curves are a theoretical prediction by Fröyland.

Fig. 12: Contributions to the π^0 photoproduction cross section for 6 GeV photons polarized normal to and parallel to the reaction plane, have been plotted separately in $\mu b/(\mathrm{GeV}/c)^2$ versus $|t|$ in $(\mathrm{GeV}/c)^2$.

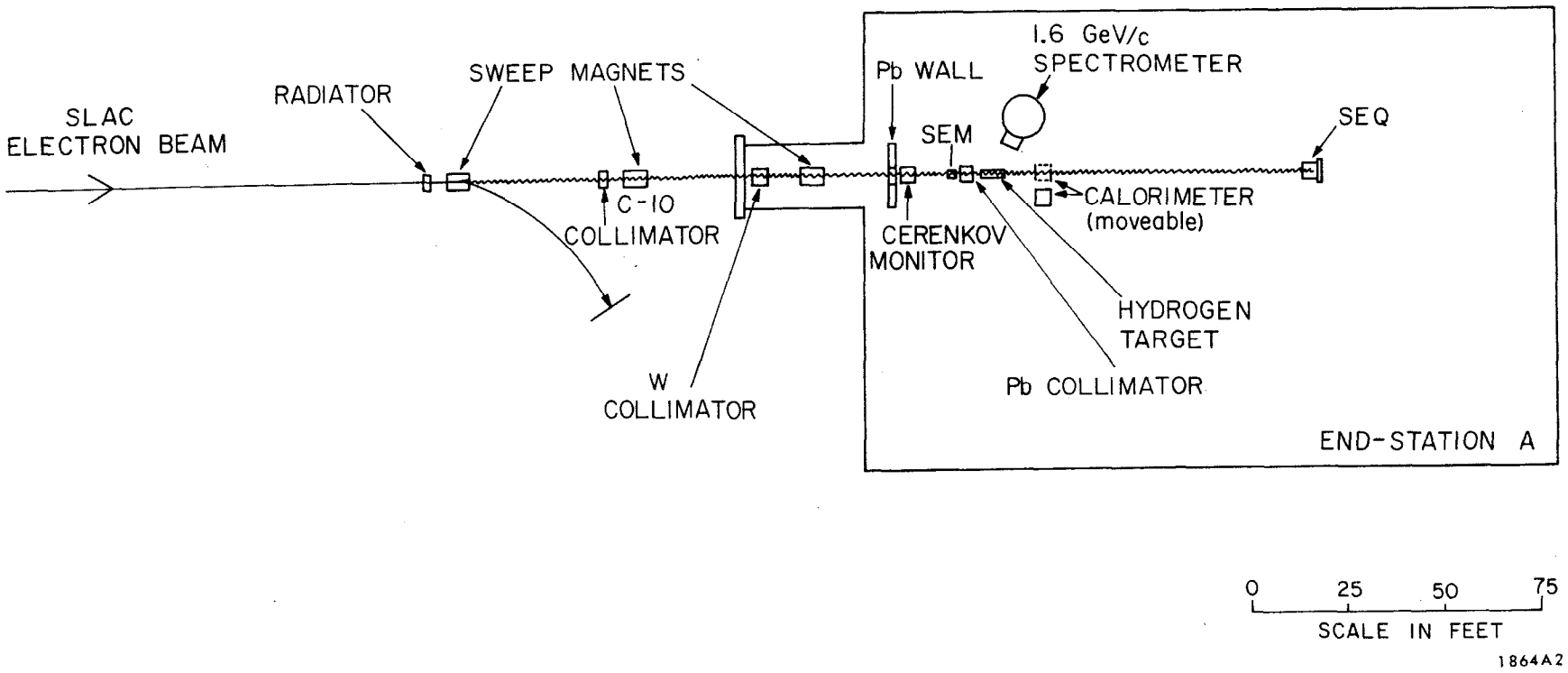
SLAC
ELECTRON BEAM
RADIATOR
SWEEP MAGNETS
C-10
COLLIMATOR
W
COLLIMATOR
Pb WALL
1.6 GeV/c
SPECTROMETER
SEM
SEQ
CALORIMETER
(moveable)
CERENKOV
MONITOR
HYDROGEN
TARGET
Pb COLLIMATOR
END-STATION A
0
25
50
75
SCALE IN FEET
1864A2

Fig. 1

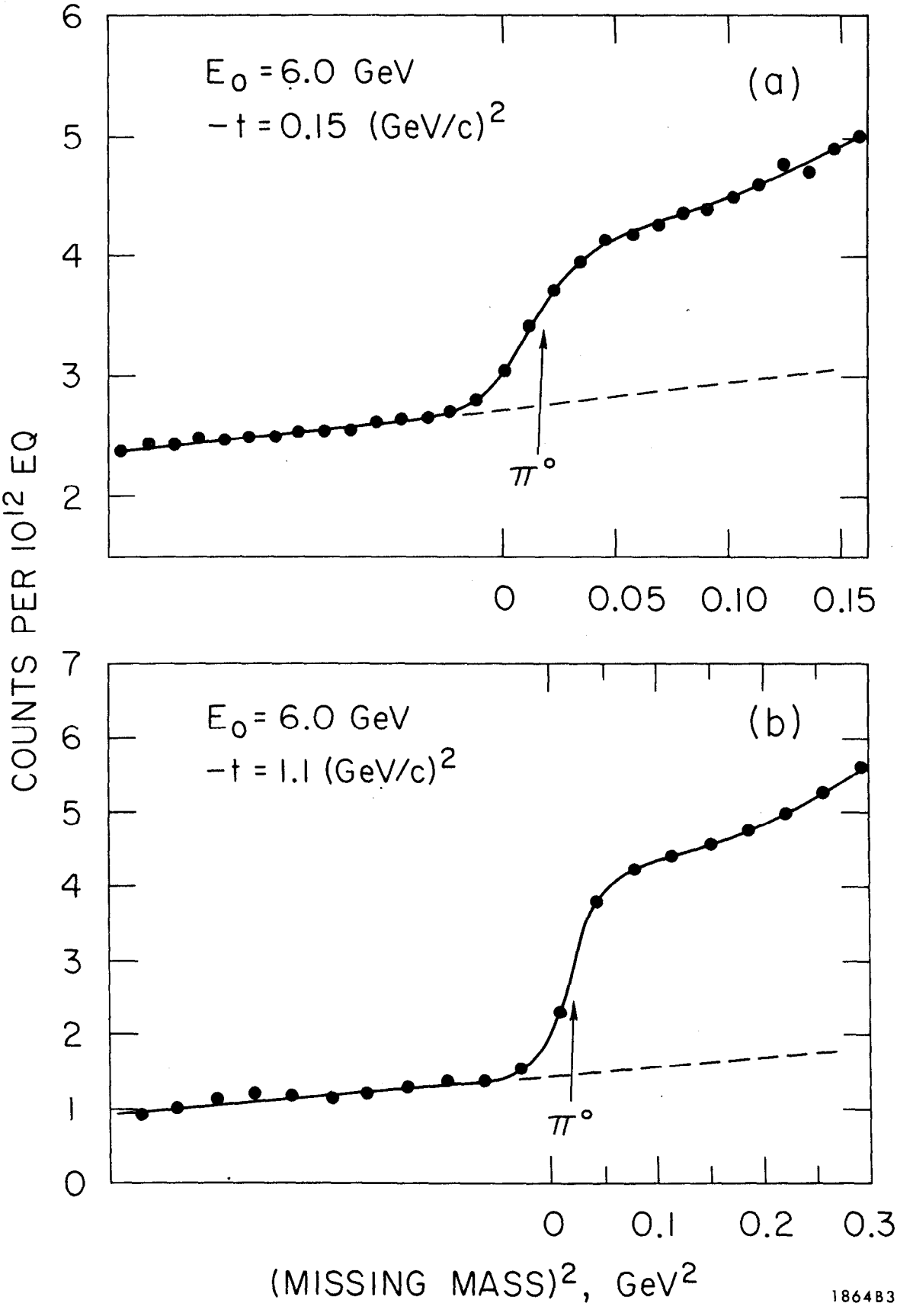
$E_0 = 6.0$ GeV
$-t = 0.15$ (GeV/c)^2
(a)
π^0
$E_0 = 6.0$ GeV
$-t = 1.1$ (GeV/c)^2
(b)
π^0
COUNTS PER 10^{12} EQ
(MISSING MASS)^2, GeV^2
1864B3

Fig. 2

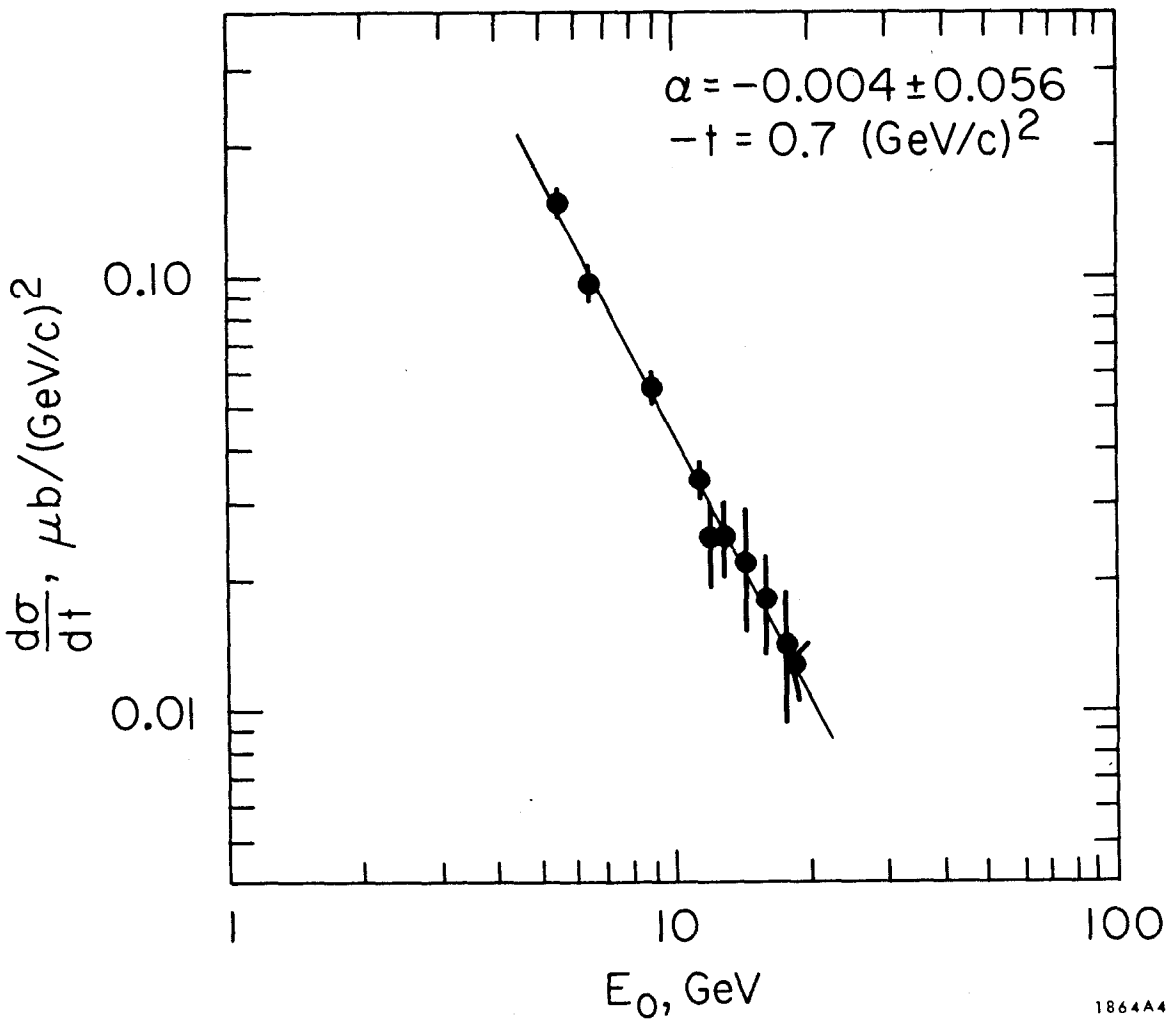
α = −0.004 ± 0.056
−t = 0.7 (GeV/c)²
0.10
0.01
dσ/dt, μb/(GeV/c)²
1
10
100
E₀, GeV
1864A4

Fig. 3

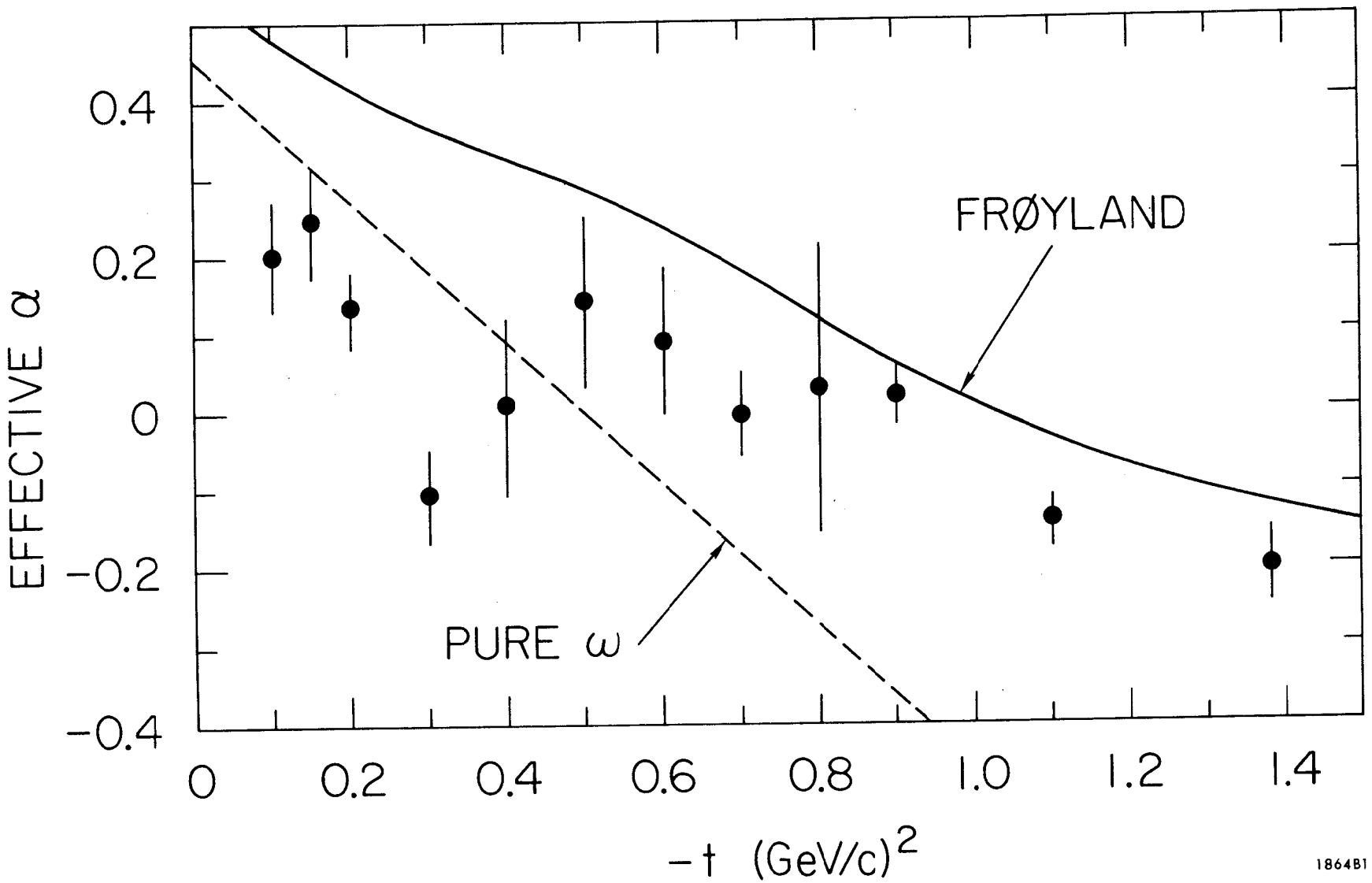
EFFECTIVE α
0.4
0.2
0
-0.2
-0.4
0
0.2
0.4
0.6
0.8
1.0
1.2
1.4
-t (GeV/c)²
FRØYLAND
PURE ω
1864B1

Fig. 4

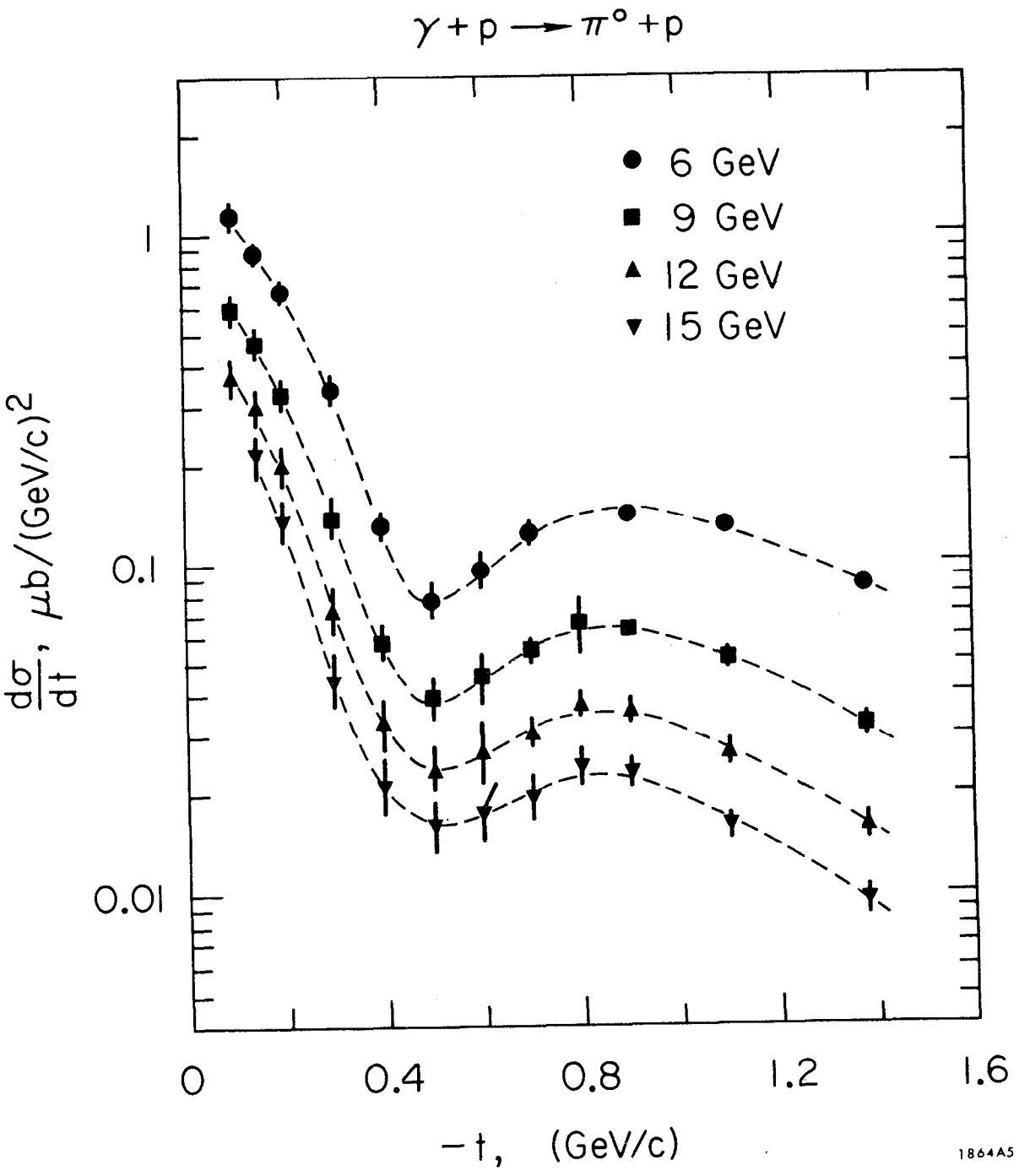
γ + p → π° + p
6 GeV
9 GeV
12 GeV
15 GeV
1
0.1
0.01
dσ/dt, μb/(GeV/c)²
0
0.4
0.8
1.2
1.6
−t, (GeV/c)
1864A5

Fig. 5

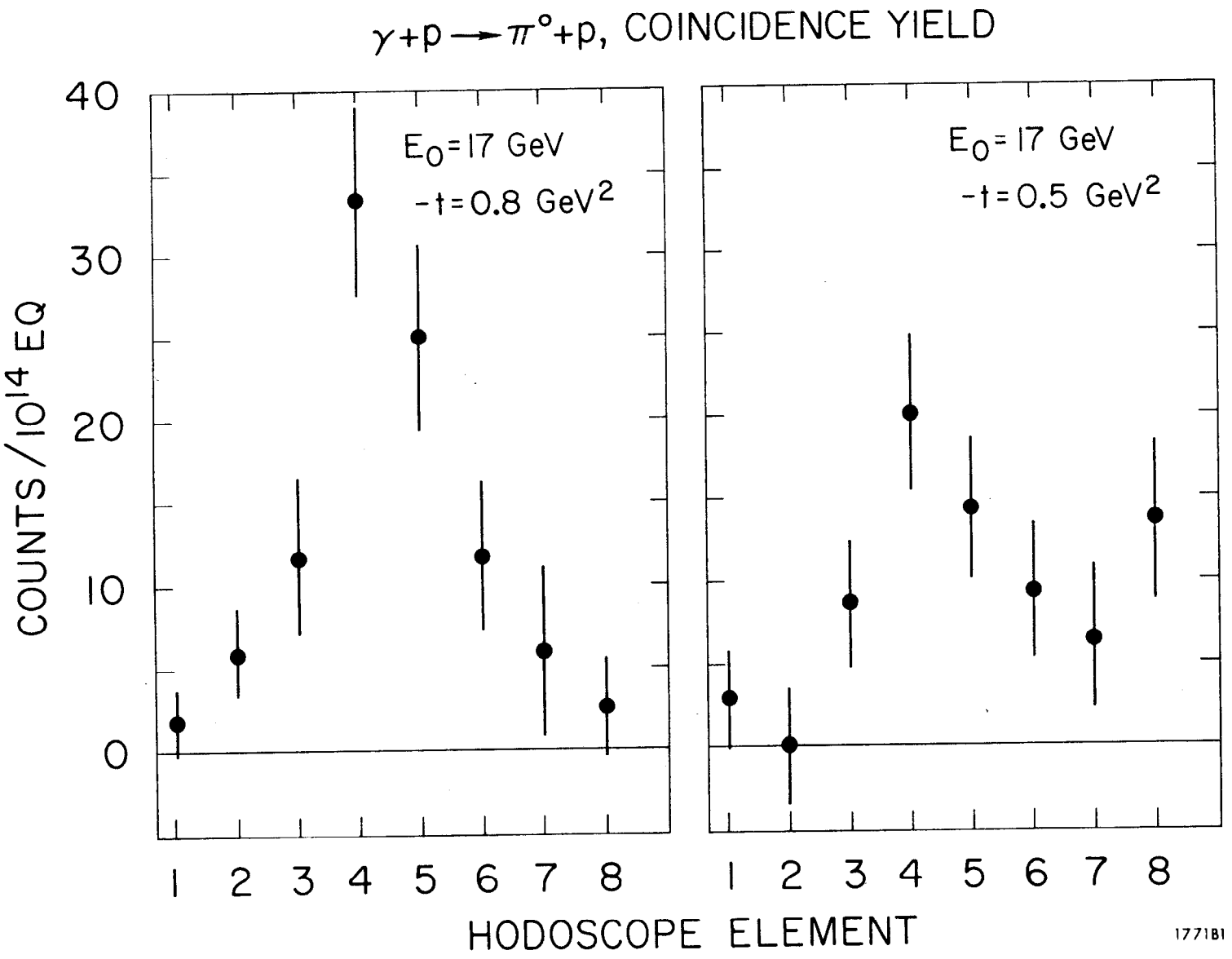
γ+p → π°+p, COINCIDENCE YIELD
E0 = 17 GeV
-t = 0.8 GeV²
E0 = 17 GeV
-t = 0.5 GeV²
COUNTS / 10¹⁴ EQ
0
10
20
30
40
1 2 3 4 5 6 7 8
1 2 3 4 5 6 7 8
HODOSCOPE ELEMENT
1771B1

Fig. 6

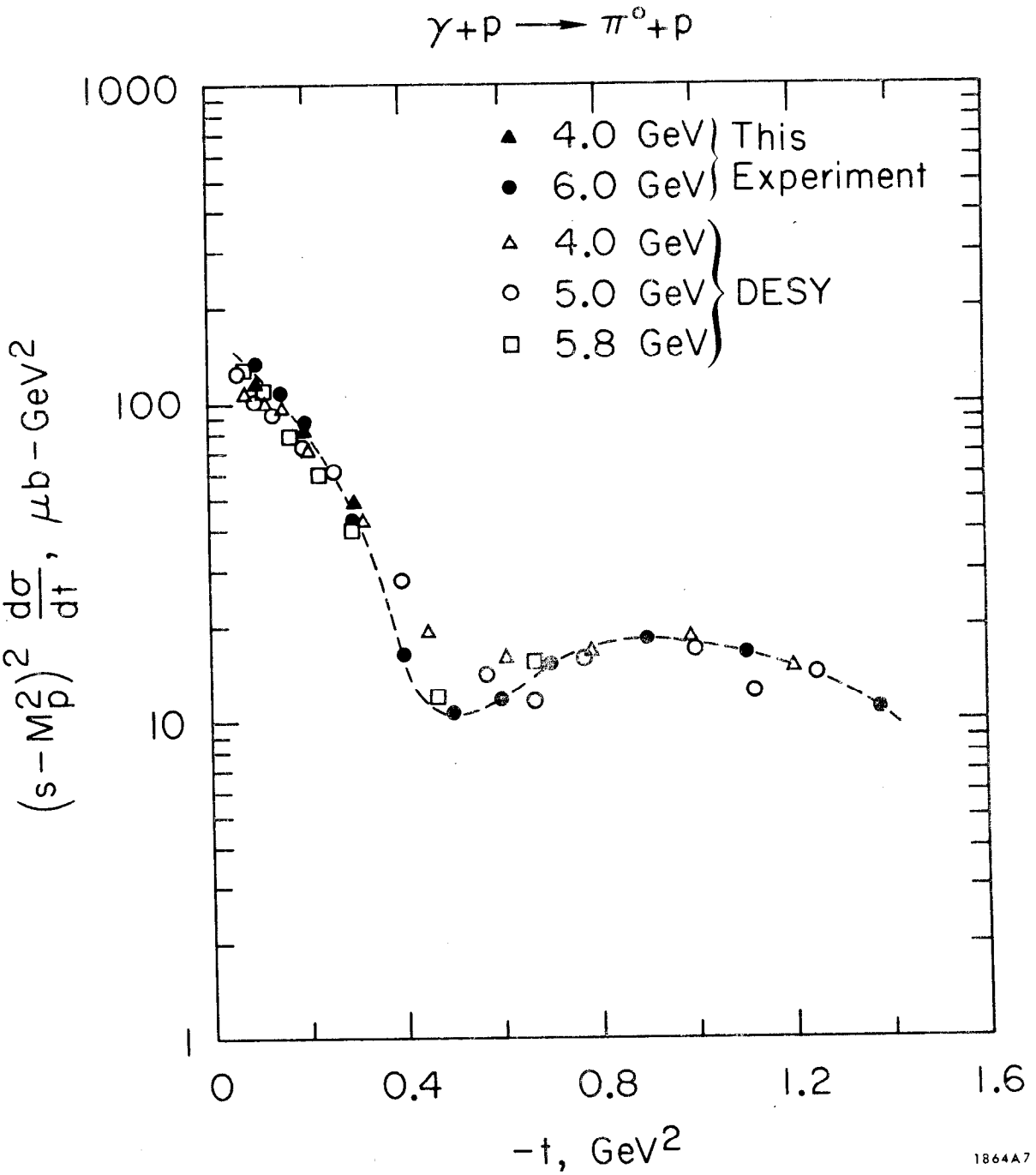
γ+p ⟶ π°+p
1000
100
10
1
0
0.4
0.8
1.2
1.6
−t, GeV²
(s−M²p)² dσ/dt, μb−GeV²
4.0 GeV
6.0 GeV
This Experiment
4.0 GeV
5.0 GeV
5.8 GeV
DESY
1864A7

Fig. 7

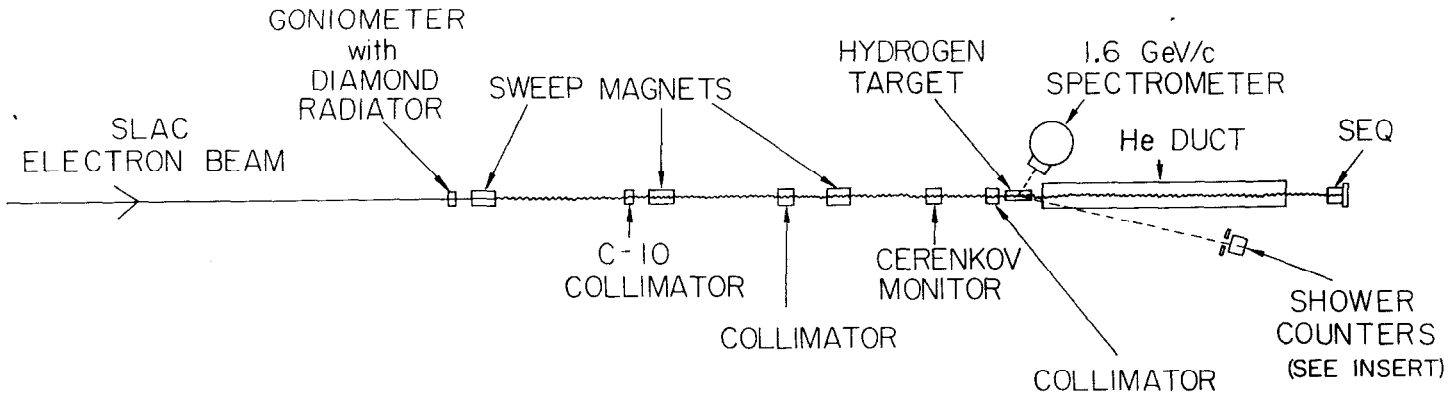
GONIOMETER
with
DIAMOND
RADIATOR
SWEEP MAGNETS
HYDROGEN
TARGET
1.6 GeV/c
SPECTROMETER
SLAC
ELECTRON BEAM
He DUCT
SEQ
C-10
COLLIMATOR
CERENKOV
MONITOR
COLLIMATOR
COLLIMATOR
SHOWER
COUNTERS
(SEE INSERT)

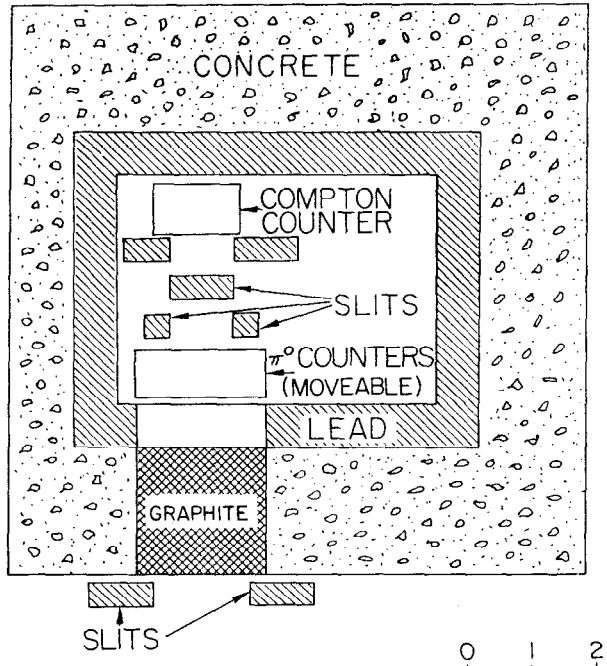
CONCRETE
COMPTON
COUNTER
SLITS
π° COUNTERS
(MOVEABLE)
LEAD
GRAPHITE
SLITS
0 1 2
SCALE IN FEET

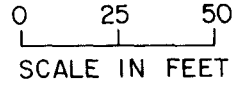
0 25 50
SCALE IN FEET

1728A3

Fig. 8

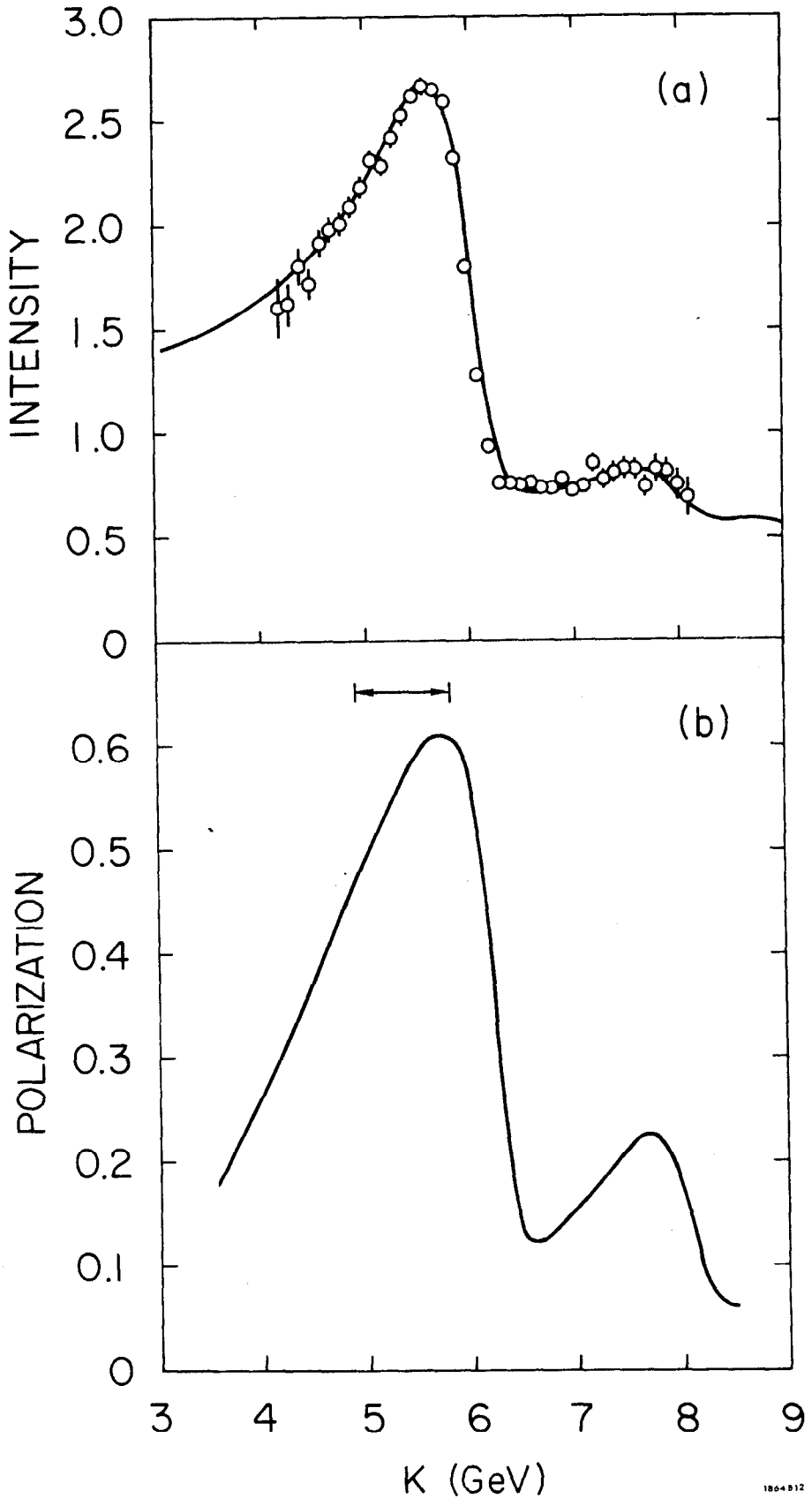
3.0
2.5
2.0
1.5
1.0
0.5
0
INTENSITY
(a)
(b)
0.6
0.5
0.4
0.3
0.2
0.1
0
POLARIZATION
3
4
5
6
7
8
9
K (GeV)
1864B12

Fig. 9

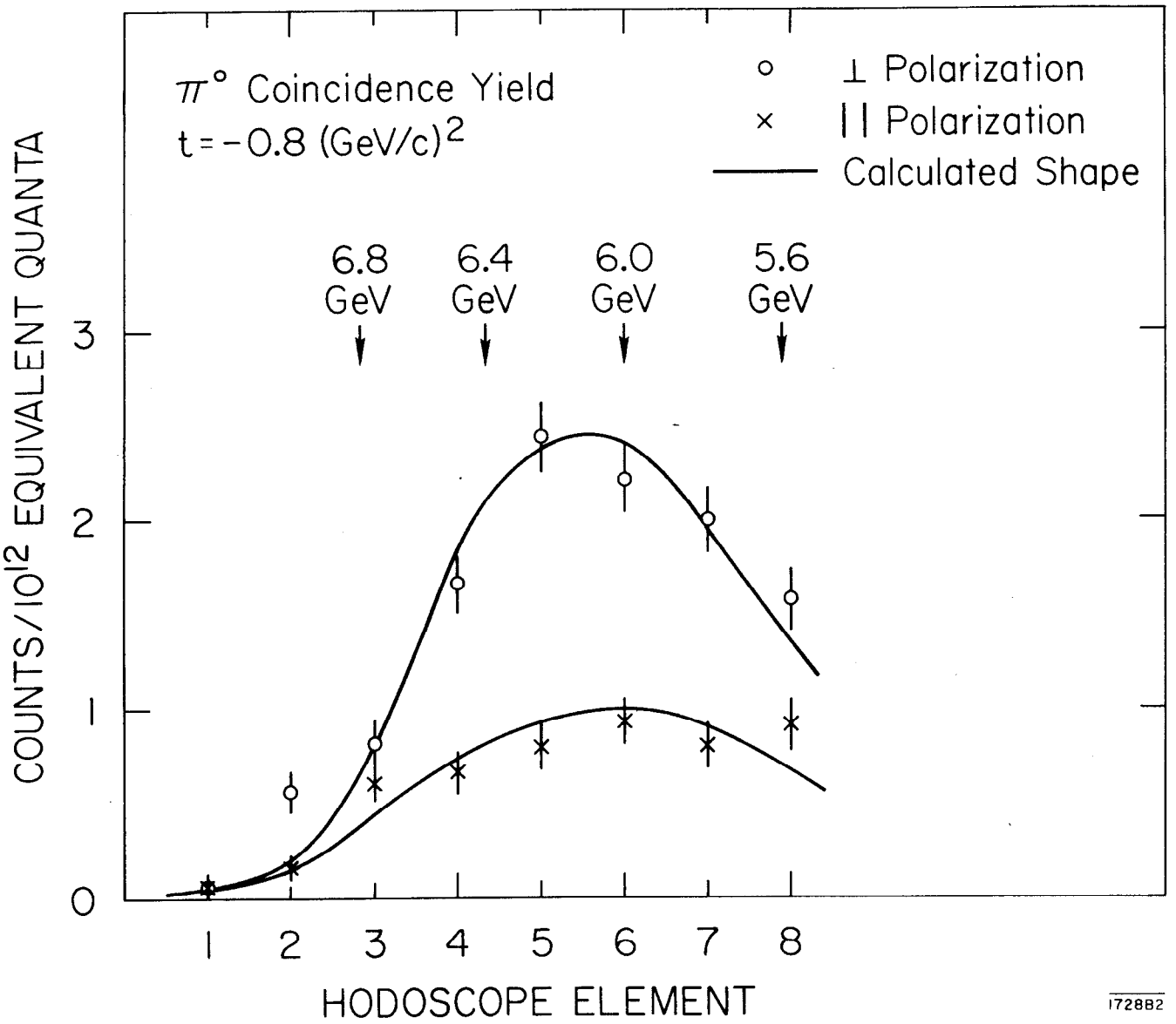
π° Coincidence Yield
t = −0.8 (GeV/c)²
⊥ Polarization
|| Polarization
Calculated Shape
6.8 GeV
6.4 GeV
6.0 GeV
5.6 GeV
COUNTS/10¹² EQUIVALENT QUANTA
0
1
2
3
1
2
3
4
5
6
7
8
HODOSCOPE ELEMENT
172882

Fig. 10

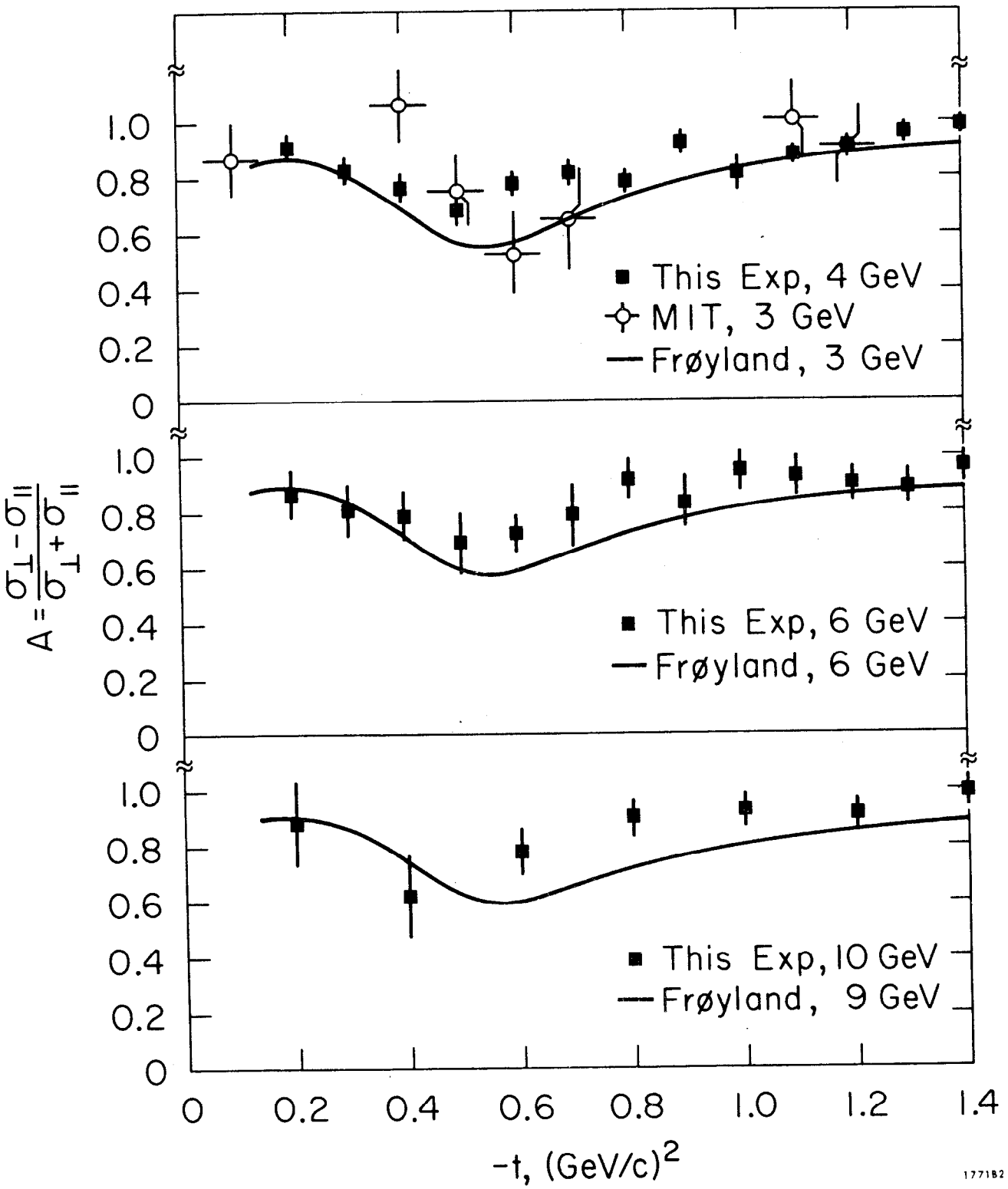
$A = \frac{\sigma_\perp - \sigma_\parallel}{\sigma_\perp + \sigma_\parallel}$
1.0
0.8
0.6
0.4
0.2
0
This Exp, 4 GeV
MIT, 3 GeV
Frøyland, 3 GeV
This Exp, 6 GeV
Frøyland, 6 GeV
This Exp, 10 GeV
Frøyland, 9 GeV
0
0.2
0.4
0.6
0.8
1.0
1.2
1.4
$-t$, (GeV/c)^2
177182

Fig. 11

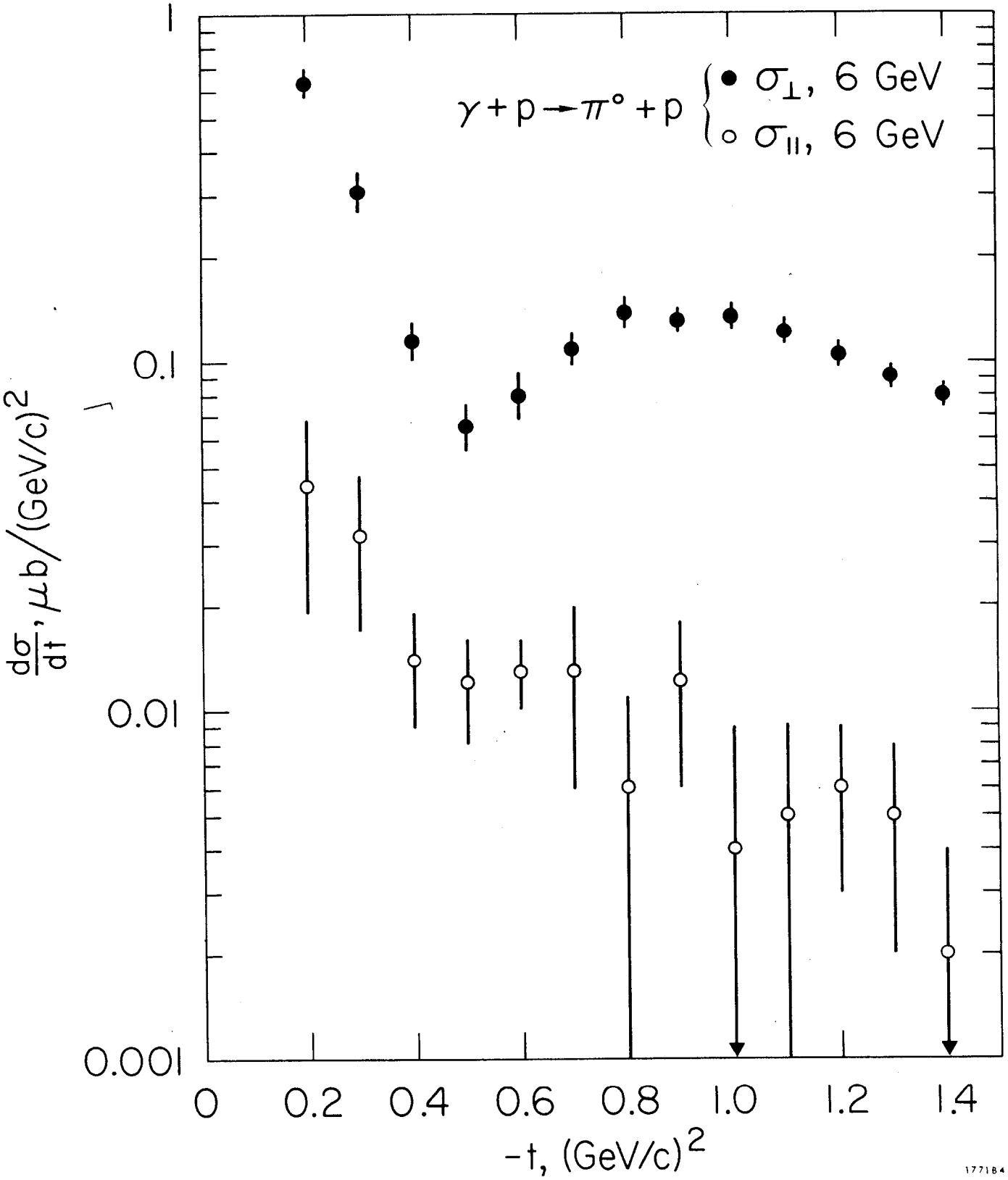
$\gamma + p \rightarrow \pi^\circ + p$
$\bullet\ \sigma_\perp$, 6 GeV
$\circ\ \sigma_{11}$, 6 GeV
$\frac{d\sigma}{dt}$, $\mu b/(GeV/c)^2$
1
0.1
0.01
0.001
0
0.2
0.4
0.6
0.8
1.0
1.2
1.4
$-t$, $(GeV/c)^2$
177184

Fig. 12